Kybernetika

Juan Carlos Cortés López; Ana Navarro-Quiles; Štěpán Papáček; Cristina Pérez Diukina

From deterministic to probabilistic modeling of algal growth under light/dark cycles: A method for density computation

Kybernetika, Vol. 62 (2026), No. 4, 618–642

Persistent URL: http://dml.cz/dmlcz/153777

Terms of use:

© Institute of Information Theory and Automation AS CR, 2026

Institute of Mathematics of the Czech Academy of Sciences provides access to digitized documents strictly for personal use. Each copy of any part of this document must contain these *Terms of use*.



This document has been digitized, optimized for electronic delivery and stamped with digital signature within the project *DML-CZ: The Czech Digital Mathematics Library* http://dml.cz

KYBERNETIKA — VOLUME *62* (2026), NUMBER 4, PAGES 618–642

FROM DETERMINISTIC TO PROBABILISTIC MODELING OF ALGAL GROWTH UNDER LIGHT/DARK CYCLES: A METHOD FOR DENSITY COMPUTATION

Juan Carlos Cortés López, Ana Navarro-Quiles, Štěpán Papáček and Cristina Pérez Diukina

This work addresses the modeling of algal growth under intermittent light conditions by extending the deterministic Photosynthetic Factory (PSF) model into a probabilistic framework. Motivated by experimental evidence that the frequency of light/dark cycles is not constant due to the inherent randomness of hydrodynamic mixing and other physical processes, the PSF model, representing one of the widely used photosynthetic-unit-based models, is first reduced to a single ordinary differential equation and then reformulated as a random differential equation, where the cycle period is treated as a continuous random variable.

A computationally relevant contribution of this study is the partition of the time domain for a piece-wise transformation method that enables the analytical computation of probability density functions for central quantities such as the proportion of active photosynthetic units and the average growth rate. A key contribution of this study is the development of a recursive transformation method that enables the analytical computation of probability density functions for central quantities such as the proportion of active photosynthetic units and the average growth rate. This method leverages the structure of the reduced PSF model and the piecewise nature of the input signal to propagate uncertainty through the system. Beyond computational considerations, a key advantage of the approach is that it provides direct access to the probability density functions and their analytical properties, which are generally not available from Monte Carlo simulations alone. This method leverages the structure of the reduced PSF model and the piecewise nature of the input signal to efficiently propagate uncertainty through the system, avoiding the computational burden of Monte Carlo simulations.

Numerical experiments illustrate how uncertainty in cycle frequency can influence both transient and long-term system behavior, and how the proposed approach allows for accurate quantification of these effects. The resulting framework offers a tractable and interpretable way to incorporate randomness into biological models of light-driven growth, with potential applications in the design and analysis of photobioreactors operating under variable environmental conditions.

Keywords: uncertainty, probability density function, random process, random differential equations, photosynthetic factory model, light/dark cycles, algal growth

Classification: 93C10, 37N25, 34F05

DOI: 10.14736/kyb-2026-4-0618

1. INTRODUCTION AND MOTIVATION

In biotechnological applications, the continuous cultivation of microalgae is pivotal for a scalable production of biofuels, feed, and the synthesis of bioactive compounds for pharmaceutical and nutraceutical use [12, 14, 22]. Among available cultivation systems, closed photobioreactors offer enhanced control over environmental conditions and reduced contamination risk, though at a higher operational cost. Therefore, improving energy efficiency in these systems is essential to ensure their viability in industrial settings [22].

Photosynthetic microalgae are highly sensitive to both the availability and variability of light, which in natural and engineered systems often fluctuates due to hydrodynamic mixing and other physical effects [24]. Experimental and theoretical studies have shown that certain species can maintain optimal growth under intermittent light exposure, but only when the frequency of light/dark cycles remains within specific limits that depend on the experimental setup and species [10, 16]. Furthermore, the inclusion of dark periods, particularly at sufficiently high frequencies [13, 23], can help cells recover from photoinhibition. These insights highlight the importance of modeling light fluctuations realistically when studying microalgae growth. Here, we highlight a family of phenomenological photosynthetic-unit-based models formulated as a deterministic system of Ordinary Differential Equations (ODEs), well suited to modeling algal growth under light/dark cycles [13, 20]. A special place within this family belongs to the widely used Photosynthetic Factory (PSF) model, introduced in 1988 by Eilers and Peeters [7], enhanced in 2001 by Merchuk and Wu [13, 25], and further studied in this journal in 2007 as a single input bilinear system [16].

Given empirical evidence that the frequency of light exposure perceived by microalgae cells is subject to random fluctuations [6], purely deterministic models either fail to capture the resulting variability in growth or require running a computationally expensive CFD (Computational Fluid Dynamics) code to assess the irradiance histories of thousands of cells and subsequently performing Monte Carlo simulations [9] or random-walk simulations.[1] To address this limitation, we extend the PSF model by formulating it within a Random Differential Equation (RDE) framework [15, 21]. With this approach, we can naturally incorporate randomness into the light/dark cycle frequency, thereby reflecting the inherent uncertainty of the photobioreactor conditions caused by turbulent mixing and other dynamic factors that remain too complex to describe in a deterministic framework. Moreover, working with RDEs enables the extension of certain deterministic results to a probabilistic setting. The inclusion of randomness in light fluctuation dynamics also accounts for the scarcity of data on mixing processes, cell trajectories, and flow speeds in photobioreactors, while acknowledging that the model itself is necessarily a simplification of reality.

We investigate how different rates of alternation between light and dark periods (light/dark cycles), where the duration of the cycle is considered random, impact the growth of microalgae. Specifically, we employ the Random Variable Transformation (RVT) technique [4, 21], which enables the derivation of the probability density functions

[1] Alternatively, an Eulerian formulation can be implemented via a user-defined function (UDF) in a commercial CFD solver, allowing an arbitrary local reaction (source) term to be prescribed in each finite contol volume [18].

for key model variables (e. g., the proportion of active photosynthetic units and the average growth rate). Furthermore, RDEs leverage existing deterministic insights from the extensive deterministic literature available, allowing us to build upon established models while accounting for the randomness.

This work extends [2]. While the previous study focused on the path-wise behaviour of the PSF model and on expectation-based quantities, the present work provides a full probabilistic characterization of the solution. In particular, we derive and analyse the probability distributions associated with the model outputs, thereby obtaining information that cannot be captured through sample paths or mean values alone. Furthermore, we investigate how different modelling assumptions for the distribution of the light/dark cycles affect the resulting productivity distribution.

To assess the impact of the cycle duration distribution on system dynamics, we conduct computational simulations. By exploring various statistical distributions for the random cycle durations, we examine how uncertainty in perceived light frequency influences both short and long-term behavior of the photosynthetic factory. Our findings shed light on the role of fluctuating light regimes in microalgae cultivation and may inform strategies to optimize biotechnological processes that depend on photosynthetic microorganisms.

The paper is structured as follows: Section 2 provides a brief overview of the deterministic PSF model, including its calibration to data and a sensitivity analysis. In Section 3, we introduce the random PSF model, describe how the model is randomized, and present some analytical results for the first probability density function (1-PDF) of the solution stochastic process, which is just its PDF at every time instant. Section 4 contains numerical examples illustrating the 1-PDF of the solution stochastic process and the corresponding growth rate. Finally, the main conclusions are summarized in the last section.

2. DETERMINISTIC PSF MODEL

2.1. PSF Model Description and its Fast Reduction

This study builds upon the PSF model introduced by Eilers and Peeters [7], in which the so-called photosynthetic unit (PSU) undergoes transitions among the three states, denoted as: *resting* (x_{R}), *active* (x_{A}), and *inhibited* (x_{B}). The states are dimensionless and can be interpreted as the proportion of cells in that condition. The transitions among states are described by a system of three ODEs. Two transitions (namely *light reactions* and a *photoinhibition* process) are driven by the photosynthetically active radiation (PAR) or irradiance $I(t)$ (with corresponding parameters α and β). Two transition rates (namely *dark reactions* and a *photoinhibition recovery* process) are modeled by the constant parameters γ and δ.

The PSF model dynamics can be written in matrix form as

$$\begin{bmatrix} \dot{x}_{\mathrm{R}} \\ \dot{x}_{\mathrm{A}} \\ \dot{x}_{\mathrm{B}} \end{bmatrix} = \begin{bmatrix} 0 & \gamma & \delta \\ 0 & -\gamma & 0 \\ 0 & 0 & -\delta \end{bmatrix} \begin{bmatrix} x_{\mathrm{R}} \\ x_{\mathrm{A}} \\ x_{\mathrm{B}} \end{bmatrix} + I(t) \begin{bmatrix} -\alpha & 0 & 0 \\ \alpha & -\beta & 0 \\ 0 & \beta & 0 \end{bmatrix} \begin{bmatrix} x_{\mathrm{R}} \\ x_{\mathrm{A}} \\ x_{\mathrm{B}} \end{bmatrix}. \tag{1}$$

The PSF model is completed by introducing a macroscopic quantity μ (*specific growth*

rate) that links the internal PSF state dynamics to the μ, defined as $\mu := \dot{c}_x/c_x$, where c_x denotes the microbial cell concentration. According to [7], the (instantaneous) rate of photosynthetic production μ is proportional to the flux of transitions from the activated state to the resting state:

$$\mu = \kappa\gamma x_{\mathrm{A}} \ , \tag{2}$$

where the dimensionless proportionality constant κ is introduced as the fifth PSF model parameter.

As follows, similarly to the procedure presented in [17], i. e., employing a suitable re-parametrization and taking into account that the PSF model states form the probabilistic vector whose components sum to one ($x_{\mathrm{R}} + x_{\mathrm{A}} + x_{\mathrm{B}} = 1$), we opt for describing only two states, namely x_{A} and x_{B}. Then, the corresponding ODE system is expressed as

$$\frac{1}{q_4}\begin{bmatrix} \dot{x}_{\mathrm{A}}(t) \\ \dot{x}_{\mathrm{B}}(t) \end{bmatrix} = \begin{bmatrix} -q_2(1+q_5) & 0 \\ 0 & -\frac{q_5}{q_2(1+q_5)} \end{bmatrix}\begin{bmatrix} x_{\mathrm{A}}(t) \\ x_{\mathrm{B}}(t) \end{bmatrix} + u(t)\begin{bmatrix} -(1+q_5) & -1 \\ q_5 & 0 \end{bmatrix}\begin{bmatrix} x_{\mathrm{A}}(t) \\ x_{\mathrm{B}}(t) \end{bmatrix}, \tag{3}$$

where the new parameters $q_i,\ i \in \{1,2,3,4,5\}$ and the dimensionless normalized irradiance $u(t) = I(t)/q_1$, replace the original Eilers and Peeters parametrization, cf. [7]. All five re-parameterized model parameters are listed in Table 1, together with their relation to the original ones, cf. [25]. Note that the new parameters are separated in such a manner that the first three concern the steady-state behavior, while the remaining two reflect the (fast) dynamics of the light reactions and the (slow) dynamics of photoinhibition.

Parameter	Unit	Experimental value	Mapping relation
q_1	μE m^{-2} s^{-1}	2.5043×10^2	$\sqrt{\frac{\gamma\delta}{\alpha\beta}}$
q_2	dimensionless	3.02×10^{-1}	$\sqrt{\frac{\alpha\beta\gamma}{\delta(\alpha+\beta)^2}}$
q_3	s^{-1}	1.765×10^{-4}	$\kappa\gamma\sqrt{\frac{\alpha\delta}{\beta\gamma}}$
q_4	s^{-1}	4.825×10^{-1}	αq_1
q_5	dimensionless	2.99741×10^{-4}	β/α

Tab. 1: Model parameters for the re-parametrized PSF model as described in [17] along with units and experimental values according to data for *Porphyridium* sp. [25].

In practical settings, especially in industrial environments, it is nearly impossible to maintain uniform, continuous light exposure across the entire system [24]. To improve homogeneity, mechanical mixing is commonly employed (e. g., by bubbling), which causes the irradiance perceived by individual cells to become intermittent and periodic. This modulation is typically modeled using a square wave rather than a sinusoidal signal, as light intensity decays rapidly due to Lambert-Beer's Law.[2]

[2]One exception is worth noting: in the laboratory photobioreactor FMT 150 made by Photon Systems Instruments, Czech Republic (www.psi.cz), the input irradiance can be imposed directly (e. g., as a harmonic function). This system combines cultivation and online monitoring and enables dynamic regulation of operating conditions for PSF parameter estimation [19].

When the normalized irradiance input $u(t)$ is represented as a square wave with period h, the signal takes the form

$$u(t) = \begin{cases} u_a := I_a/I_{\text{opt}}, & t \in ((i-1)h, (i-1)h + rh), \\ u_b := I_b/I_{\text{opt}}, & t \in ((i-1)h + rh, ih), \end{cases} \quad i \in \mathbb{N}, \tag{4}$$

where $r \in (0,1)$ is the dark duty cycle, I_a and I_b denote the irradiance levels during the dark and light phases, respectively, and $I_{\text{opt}} = q_1$ is the optimal constant irradiance identified in a small laboratory cultivator with low density algal culture and homogeneous light conditions. This piecewise-constant representation introduces stiffness and distinct timescales into the system, making the full ODE model difficult to analyze both analytically and numerically [16]. To address this, a fast-timescale reduction has been proposed, yielding a single ODE that accurately approximates the dynamics of the active state x_{A}, provided the cycle period satisfies $h < \mathrm{e}^4$, corresponding to sufficiently fast light-dark cycling [5, 17]. The reduced model is given by

$$\dot{x}_{\text{A}}(t) = -q_4 \left[u(t) + q_2\right] x_{\text{A}}(t) + q_4 u(t) \left[1 - x_{\text{B}}^{\text{ss}}(u_{\text{av}})\right], \tag{5}$$

where the steady-state value of the inhibited state in the full PSF model under constant irradiance u is

$$x_{\text{B}}^{\text{ss}}(u) = \frac{u^2}{u^2 + u/q_2 + 1}, \tag{6}$$

and the average irradiance over a cycle is given by

$$u_{\text{av}} := \frac{1}{h} \int_0^h u(t)\, \mathrm{d}t.$$

The initial condition problem for the reduced model is straightforward to solve numerically, as it involves a first-order linear differential equation. The solution can be obtained using the integrating factor method, yielding

$$x_{\text{A}}(t) = \frac{\int_0^t \left(\mathrm{e}^{\int_0^s q_4(u(w)+q_2)\, \mathrm{d}w} (q_4 u(s)[1 - x_{\text{B}}^{ss}(u_{\text{av}})]) \right) \mathrm{d}s + x_0}{\mathrm{e}^{\int_0^t q_4(u(s)+q_2)\, \mathrm{d}s}}, \tag{7}$$

where x_0 is the initial condition. Note that u_{av} is constant since it depends only on the cycle-averaged irradiance. For square-wave irradiance with period $h < \mathrm{e}^4$, solutions $x_{\text{A}}(t)$ of the reduced model converge exponentially fast to a unique h-periodic orbit, independently of initial conditions, as shown in [5, 16]. Consequently, cycle-averaged quantities can be defined unambiguously. Furthermore, for $h < e^4$, numerical simulations have shown that the fast PSF model reduction is a very good approximation of the full model. The analysis of the PSF model for periods greater than this would necessitate the slow model reduction. Our goal, however, is to investigate case scenarios that lead to a relatively high production yield, which is usually not feasible for such high values of h [3, 13]. We will thus set this as an upper limit for our analysis.

This reduced model is particularly relevant for optimizing microalgal production, as the specific growth rate can be deduced directly from $x_{\text{A}}(t)$ using the relation (2), see

also [7, 25]. Once $x_{\mathrm{A}}(t)$ reaches its periodic regime after K cycles, the cycle-averaged growth rate is given by

$$\mu(h) = \kappa\gamma \frac{1}{h} \int_{Kh}^{(K+1)h} x_{\mathrm{A}}(t)\, \mathrm{d}t, \tag{8}$$

where $\kappa = 3.647 \times 10^{-3}$ for *Porphyridium* sp. [25].[3] Since the magnitude of $\mu(h)$, given by (8), is typically small, the productivity of the system p is instead defined

$$p(h) = \frac{\mu(h)}{\mu_o(u_{\mathrm{av}})}, \tag{9}$$

with $\mu_o(u_{\mathrm{av}}) = \kappa\gamma \frac{u_{\mathrm{av}}}{q_2(1+q_5)(u_{\mathrm{av}}^2+u_{\mathrm{av}}/q_2+1)} = q_3 \frac{u_{\mathrm{av}}}{(u_{\mathrm{av}}^2+u_{\mathrm{av}}/q_2+1)}$ being the specific growth rate of the (nonreduced) PSF model with a constant input u_{av} [17].

2.2. Model calibration and sensitivity analysis of the average growth rate

We use the experimental data reported in [25] to assess how the reduced-model definition of μ aligns with observed growth rates. To emphasize the dependence of μ and x_{A} on the light/dark cycle ratio r, we write $\mu(h) = \mu(h; r)$ and $x_{\mathrm{A}}(t) = x_{\mathrm{A}}(t; r)$. Note that in [25] the authors define the specific growth rate μ with an additional maintenance constant M_e (with units h^{-1}), which reflects experimental observations that biomass growth rate may be negative when the irradiance is below the so-called light compensation point. [4] In that case, (2) is modified to

$$\mu = \kappa\gamma\, x_{\mathrm{A}}(t) - M_e.$$

In the notation of [25], the total cycle time t_c corresponds to our h, while the light interval t_ℓ satisfies

$$t_\ell \;=\; h\,(1-r)\,.$$

Denoting by $\mu_p(h; r)$ the specific growth rate reported in [25], we convert to our units via

$$\mu(h; r) \;=\; \frac{\mu_p(h; r) + M_e}{3600}\,.$$

By fitting the reduced model at the experimental period $h = 45$s, with irradiance levels $I_a = 0$ μmol photons $\mathrm{m}^{-2}\mathrm{s}^{-1}$, $I_b = 220$ μmol photons $\mathrm{m}^{-2}\mathrm{s}^{-1}$, we recover a curve nearly identical to Figure 5 of [25] as can be seen in Figure 1. Note that here we have not included the data points corresponding to the continuous light set-up obtained in the experiment by using a very thin layer of algae since our study is restricted to intermittent illumination regimes with $r \in (0, 1)$. This agreement is consistent with the results of [5], in which it was shown that the reduced model closely approximates the full model for cycle lengths $h < \mathrm{e}^4$ s ≈ 55 s (which is greater than the experimental period of 45 s).

Using the experimental parameters reported in [25] and fixing $r = 0.5$, the solution $x_{\mathrm{A}}(t; 0.5)$ rapidly reaches a quasi-steady state, as shown in Figure 2.

[3] The mapping relation $\kappa\gamma = q_2 q_3(1 + q_5)$, linking the original parameters to the re-parameterized set, can be substituted into (8) and applied subsequently whenever needed.

[4] Nevertheless, as our focus is solely on the effects of h and r on μ, we further neglect the maintenance term here.

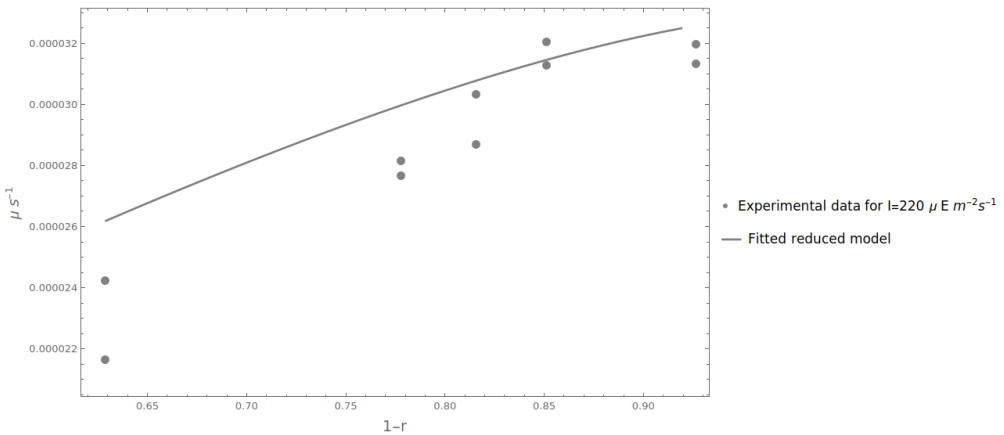


Fig. 1: Plot of μ as defined in Eq. (8), using a light cycle period of $h = 45\,\mathrm{s}$, irradiance levels $I_a = 0\,\mu\mathrm{mol\ photons\,m^{-2}s^{-1}}$ (dark phase) and $I_b = 220\,\mu\mathrm{mol\ photons\,m^{-2}s^{-1}}$ (light phase). Model parameters and experimental data are taken from [25].

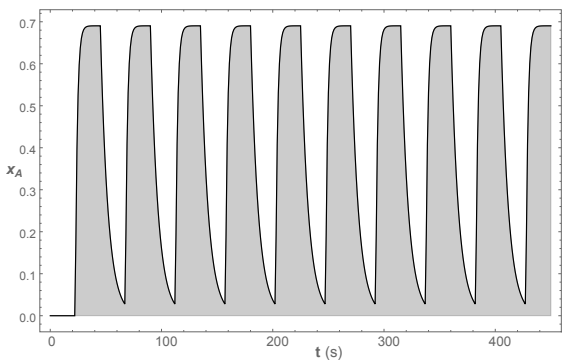


Fig. 2: Numerical solution of $x_{\mathrm{A}}(t;r)$ as given in Eq. (7), using a light cycle period of $h = 45\,\mathrm{s}$, irradiance levels $I_a = 0\,\mu\mathrm{mol\ photons}^{-1}\,m^{-2}\,s^{-1}$ (dark phase) and $I_b = 220\,\mu\mathrm{mol\ photons}^{-1}\,m^{-2}\,s^{-1}$ (light phase), with a light/dark ratio of $r = 0.5$. Model parameters are taken from [25].

We now examine how the average specific growth rate μ responds to changes in the cycle length h to emphasize its dependence on both h and the dark-time fraction r. Its elasticity with respect to h, denoted by E_h, is defined as

$$E_h(h;r) \;=\; \frac{h}{\mu(h;r)}\,\frac{\partial\,\mu(h;r)}{\partial h}\,.$$

This dimensionless elasticity quantifies the sensitivity of the average growth rate to changes in the light–dark cycle length, allowing comparison across operating regimes and providing a natural metric for process optimization.

Starting from the average growth rate expression (8), we assume that the activated-state fraction x_{A} has reached its quasi-steady regime, so that $x_{\mathrm{A}}((K{+}1)h;r) = x_{\mathrm{A}}(Kh;r)$. Applying the Leibniz rule to differentiate under the integral sign, then yields the closed-form

$$E_h(h;r) \;=\; \frac{\kappa\,\gamma}{\mu(h;r)}\left[x_{\mathrm{A}}(Kh;r) + \int_{Kh}^{(K+1)h} \frac{\partial x_{\mathrm{A}}(t;r)}{\partial h}\mathrm{d}t\right] \;-\; 1\,. \tag{10}$$

Figure 3 presents the contour map of the elasticity E_h defined in (10) over the (h,r) plane. For short cycle lengths h, E_h remains uniformly low for all values of r, indicating that small values of h robustly enhance the mean growth rate μ regardless of the dark-period fraction. As h increases, however, the sensitivity of μ to the dark interval becomes pronounced: larger values of r lead to a much steeper increase in E_h, implying that for long cycles maximizing μ requires careful control of the darkness ratio. In particular, when $r \approx 0$ (i. e. negligible darkness), E_h remains close to zero, indicating that variations in h have little influence on μ and that the system effectively behaves as if under continuous illumination. Overall, small values of h yield consistent gains in μ, whereas for large h the dependence on r becomes dominant, in agreement with the experimental results reported in [25].

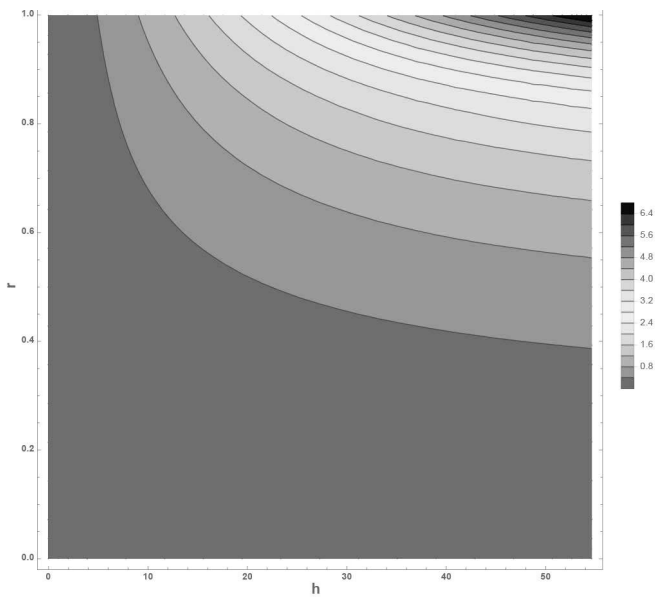


Fig. 3: Contour plots of the elasticity E_h (10) as h and r change: $h \in (0, e^4)$, $r \in (0,1)$, using irradiance levels $I_a = 0\,\mu$mol photons$^{-1}\,m^{-2}\,s^{-1}$ (dark phase) and $I_b = 220\,\mu$mol photons$^{-1}\,m^{-2}\,s^{-1}$ (light phase). Model parameters and experimental data are taken from [25].

Having described the deterministic PSF model and its simplifications, the sharp dependence of μ on h and r for large cycles suggests that intrinsic fluctuations in irradiance or physiological parameters may significantly affect productivity, motivating a stochastic

extension of the model that accounts for experimental evidence of intrinsic variability in the system parameters.

3. RANDOM MODEL

3.1. Random Reduced PSF Model

Experimental observations suggest that the frequency, f, of the hydrodynamically-induced light/dark cycle exhibits variability [6]. Since the cycle length h is simply the multiplicative inverse of f, i. e., $h = 1/f$, we will treat it as a random variable. We therefore model $H = h(\omega)$ as a continuous random variable defined on a complete probability space $(\Omega, \mathcal{F}_\Omega, \mathbb{P})$. Thus, all randomness enters the model exclusively through the parametric dependence on the random variable H. For each fixed realization $H = h(\omega)$, the system is an ordinary differential equation with piecewise continuous coefficients. Hence, the analysis is entirely pathwise and does not involve stochastic differential equations in the Itô or Stratonovich sense, but rather a family of deterministic ODEs indexed by H. For generality, we also allow the initial condition $X_0 = x_0(\omega)$ of the reduced PSF model (as introduced in Eq. (5)) is also a random variable.

More precisely, given $T > 0$, to ensure physical consistency and mathematical well-posedness of the time partition induced by $\lfloor t/h \rfloor$, we shall assume that H is bounded away from zero, $H : \Omega \to [h_0, T)$ for some $0 < h_0 < T$, where T denotes a maximal observation horizon, and $X_0 : \Omega \to (0, 1)$.

Under this setting, the deterministic differential equation (5) becomes the random differential equation (RDE):

$$\dot{X}_{\mathrm{A}}(t; H) = -\, q_4 \left[u(t; H) + q_2\right] X_{\mathrm{A}}(t; H) + q_4 u(t; H) \left[1 - x_{\mathrm{B}}^{\mathrm{ss}}\big(u_{\mathrm{av}}(H)\big)\right], \tag{11}$$

where $x_{\mathrm{B}}^{\mathrm{ss}}$ is the steady-state value of the inhibited state x_{B}, defined in (6), and q_2 and q_4 are deterministic constants introduced in Section 2. In (11), the notation $X_{\mathrm{A}}(t; H)$ and $u(t; H)$ explicitly highlights the dependence of both random quantities on the random variable H.

The randomized irradiance $u(t; H)$ is defined as:

$$u(t; H) = \begin{cases} u_a, & t \in ((i-1)H, (i-1+r)H), \\ u_b, & t \in ((i-1+r)H, iH), \end{cases} \qquad i \in \mathbb{N},\ r \in (0, 1), \tag{12}$$

with u_a and u_b, denoting the dark and light irradiance levels, respectively, making $u(t; H)$ a randomly time-modulated dichotomous signal due to its dependence on a random time partition.

Although $u(t; H)$ is random due to its dependence on H, its time average $u_{\mathrm{av}} = ru_a + (1 - r)u_b$ is independent of H, and hence remains a deterministic quantity. We therefore suppress the argument and denote it simply by u_{av}.

To simplify notation, we rewrite the RDE in Eq. (11) as:

$$\dot{X}_{\mathrm{A}}(t; H) + a(t, u(t, H)) X_{\mathrm{A}}(t; H) = b(t, u(t; H)), \tag{13}$$

where

$$\begin{aligned} a(t, u(t; H)) &= q_4 \left[u(t; H) + q_2\right], \\ b(t, u(t; H)) &= q_4 u(t; H) \left[1 - x_{\mathrm{B}}^{\mathrm{ss}}(u_{\mathrm{av}})\right]. \end{aligned}$$

The solution stochastic process is given by a mapping formally identical to the deterministic solution in (7):

$$X_{\mathrm{A}}(t;H) = \frac{X_0 + \int_0^t \nu(s,u(s;H))\, b(s,u(s;H))\,\mathrm{d}s}{\nu(t,u(t;H))}, \tag{14}$$

where

$$\nu(t,u(t;H)) = \exp\left(\int_0^t a(s,u(s;H))\,\mathrm{d}s\right). \tag{15}$$

We now apply the RVT method, [21, Ch. 2], to compute the 1-PDF of $X_{\mathrm{A}}(t)$ for a fixed t. Let $\boldsymbol{u} := (X_0, H)$ and $\boldsymbol{v} := (X_{\mathrm{A}}, H)$. Then there exists a bijective map $\boldsymbol{r} = (r_1, r_2)$ such that $\boldsymbol{v} = \boldsymbol{r}(\boldsymbol{u})$. The inverse map $\boldsymbol{s} = (s_1, s_2) := \boldsymbol{r}^{-1}$ satisfies:

$$X_0 = X_{\mathrm{A}}(t;H)\nu(t,u(t;H)) - \int_0^t \nu(s,u(s;H))b(s,u(s;H))\,\mathrm{d}s.$$

Since H is preserved, s_2 is the identity. The Jacobian determinant of the inverse map is $\nu(t,u(t;H))$, and thus the PDF becomes:

$$f_{X_{\mathrm{A}}}(x,t) = \int_0^T f_H(h) f_{X_0}\left(x\nu(t,u(t;h)) - \int_0^t \nu(s,u(s;h))b(s,u(s;h))\,\mathrm{d}s\right)\nu(t,u(t;h))\,\mathrm{d}h, \tag{16}$$

where independence of X_0 and H is assumed: $f_{X_0,H}(x_0,h) = f_{X_0}(x_0)f_H(h)$.

Note that the initial condition is retrieved when $t = 0$, since $\nu(0,u(0;h)) = 1$, $\int_0^0 \nu(s,u(s;h))\, b(s,u(s;h))\,\mathrm{d}s = 0$ and by definition $\int_{\mathbb{R}} f_H(h)\,\mathrm{d}h = 1$ and $f_{X_{\mathrm{A}}}(x,0) = f_{X_0}(x)$.

Although the expression (16) provides a closed-form representation of the 1-PDF of $X_{\mathrm{A}}(t)$, its direct numerical evaluation is computationally inefficient. Indeed, the integrating factor ν depends on the random time partition induced by H, requiring the repeated evaluation of integrals with random limits. This motivates a reformulation of the solution exploiting the piecewise-constant structure of $u(t;h)$ and considering a partition of the time domain accordingly. First, let N be fixed, which is the maximum number of periods that we are interested in simulating. Defining $J := \sum_{k=1}^{N} \mathbb{1}(kh \le t) = \lfloor t/h \rfloor$, that in the stochastic setting is a random integer-valued variable depending on H, in the deterministic setting we can rewrite the integral of the irradiance as

$$\begin{aligned}\mathcal{U}(t;h) := \int_0^t u(s;h)\mathrm{d}s = {} & J\cdot(rhu_a + (1-r)hu_b) \\ & + \mathbb{1}(Jh < t \le Jh + rh)\cdot(t - Jh)u_a \\ & + \mathbb{1}\left(t > Jh + rh\right)\cdot(rhu_a + (t - Jh - rh)u_b)\,.\end{aligned}$$

Therefore,

$$\begin{aligned} & \nu(t,u(s;h)) = \mathrm{e}^{\int_0^t a(s,u(s;h))\,\mathrm{d}s} \\ = \quad & \mathrm{e}^{\int_0^t q_4(u(s;h)+q_2)\mathrm{d}s} = \mathrm{e}^{q_4q_2t+q_4\int_0^t u(s;h)\mathrm{d}s} = \mathrm{e}^{q_4q_2t+q_4\mathcal{U}(t;h)} \end{aligned}$$

and

$$\begin{aligned} & \int_0^t \nu(s,u(s;h))b(s,u(s;h))\mathrm{d}s \\ = \quad & \underbrace{\int_0^{Jh} \nu(s,u(s;h))b(s,u(s;h))\mathrm{d}s}_{\mathrm{Int}_1} + \underbrace{\int_{Jh}^t \nu(s,u(s;h))b(s,u(s;h))\mathrm{d}s}_{\mathrm{Int}_2}, \end{aligned}$$

where the integral has been split into two parts to show the dependence on the parameter h, which, in our case, is the parameter that contains the uncertainty.

Firstly, we reformulate Int_1 by dividing the interval $[0, Jh]$ into intervals of type $I_1(i) = ((i-1)h, (i-1)h + rh)$ and $I_2(i) = ((i-1)h + rh, ih)$, for $i = 1, \ldots, J$, then

$$\begin{aligned} \mathrm{Int}_1(h) = q_4\left(1 - x_{\mathrm{B}}^{\mathrm{ss}}(u_{\mathrm{av}})\right) \sum_{i=1}^{J} \Bigg\{ & u_a \int_{(i-1)h}^{(i-1)h+rh} \nu(s,u(s;h))\mathrm{d}s \\ & + u_b \int_{(i-1)h+rh}^{ih} \nu(s,u(s;h))\mathrm{d}s \Bigg\} \end{aligned} \tag{17}$$

and

$$\begin{aligned} \mathrm{Int}_2(h) = {} & \mathbb{1}(0 \le t - Jh < rh) q_4 u_a \left(1 - x_{\mathrm{B}}^{\mathrm{ss}}(u_{\mathrm{av}})\right) \int_{Jh}^{t} \nu(s,u(s;h))\mathrm{d}s \\ & + \mathbb{1}(t - Jh \ge rh) q_4 \left(1 - x_{\mathrm{B}}^{\mathrm{ss}}(u_{\mathrm{av}})\right) \Bigg[u_a \int_{Jh}^{Jh+rh} \nu(s,u(s;h))\mathrm{d}s \\ & + u_b \int_{Jh+rh}^{t} \nu(s,u(s;h))\mathrm{d}s \Bigg]. \end{aligned} \tag{18}$$

Using again the independence of X_0 and H, together with the decompositions (17)–(18), the expression for the 1-PDF in (16) can be rewritten equivalently in terms of an expectation:

$$f_{X_A}(x,t) = \mathbb{E}_H\left[f_{X_0}\left(x\nu(t,u(t;H)) - \left(\mathrm{Int}_1(H) + \mathrm{Int}_2(H)\right)\right) \nu(t,u(t;H))\right], \; t \ge 0. \tag{19}$$

3.2. Analytical study of the critical points of the PDF of X_A

Beyond the explicit computation of the PDF of $X_A(t)$, its qualitative structure plays a central role in understanding the effects of randomness in the light–dark cycle. In particular, the number and location of the critical points of $f_{X_A}(\cdot, t)$ determine whether the active-state fraction concentrates around a single most probable value or whether multiple preferred states emerge as a consequence of variability in the cycle length. These

features reflect how fluctuations in the random parameter H are propagated through the reduced PSF dynamics and shape the distribution of photosynthetic activity at a given time. This observation motivates an analytical study of the critical points of the PDF of $X_A(t)$.

For a fixed time $t > 0$, the PDF of X_A derived in Eq. (16) can be written as

$$f_{X_A}(x,t) = \int_0^T f_H(h)\, f_{X_0}\big(xg_1(t,h) - g_2(t,h)\big)\, g_1(t,h)\,\mathrm{d}h,$$

where

$$g_1(t,h) = \mathrm{e}^{q_4 q_2 t + q_4 \mathcal{U}(t;h)}, \qquad g_2(t,h) = \int_0^t g_1(s,h)\, b(s,u(s;h))\,\mathrm{d}s. \tag{20}$$

We remark that ν (15) and g_1 (20) are equivalent, however, since g_1 benefits from a more compact notation and the partition of the integration domain, it will be used from now on. The initial condition X_0 represents a fraction of activated photosystems and therefore takes values in the interval $(0,1)$. To model its variability while preserving analytical tractability and regularity, we assume that X_0 follows a Beta distribution truncated to $[\varepsilon, 1-\varepsilon]$, with $\varepsilon > 0$. Its probability density function is given by

$$f_{X_0}(y) = \frac{y^{\alpha-1}(1-y)^{\beta-1}}{B(\alpha,\beta)\big[I_{1-\varepsilon}(\alpha,\beta) - I_\varepsilon(\alpha,\beta)\big]}\, \mathbb{1}_{[\varepsilon,\,1-\varepsilon]}(y), \qquad \alpha,\beta > 0,$$

where $I_x(\alpha,\beta) = \frac{1}{B(\alpha,\beta)} \int_0^x t^{\alpha-1}(1-t)^{\beta-1}\,\mathrm{d}t$, $x \in [0,1]$, denotes the regularized incomplete beta function, being $B(\alpha,\beta) = \int_0^1 t^{\alpha-1}(1-t)^{\beta-1}\,\mathrm{d}t$, the beta function [8]. This normalization ensures that f_{X_0} integrates to one over its support. Moreover, the truncation guarantees that f_{X_0} is continuously differentiable with bounded derivative on $[\varepsilon, 1-\varepsilon]$, a property required for the differentiation performed below.

Since the random variable H is bounded and $g_1(t,h)$ is continuous in h, the integrand admits an integrable dominating function independent of x. Differentiation under the integral sign is therefore justified by the dominated convergence theorem. The derivative of f_{X_A} with respect to x is given by

$$\frac{\mathrm{d}}{\mathrm{d}x} f_{X_A}(x,t) = \int_0^T f_H(h)\,(g_1(t,h))^2\, \frac{\mathrm{d}}{\mathrm{d}y} f_{X_0}(y)\Big|_{y = xg_1(t,h) - g_2(t,h)} \mathrm{d}h.$$

We restrict attention to values of x such that

$$y(x;t,h) := xg_1(t,h) - g_2(t,h) \in (\varepsilon, 1-\varepsilon) \subset (0,1), \quad h \in (0,T),$$

since outside this range the integrand vanishes and $f_{X_A}(x,t) = 0$.

For $y \in (\varepsilon, 1-\varepsilon)$, the derivative of the Beta density reads

$$\frac{\mathrm{d}}{\mathrm{d}y} f_{X_0}(y) = f_{X_0}(y) \left(\frac{\alpha-1}{y} - \frac{\beta-1}{1-y} \right).$$

Hence,

$$\frac{\mathrm{d}}{\mathrm{d}x} f_{X_A}(x,t) = \int_0^T f_H(h)\,(g_1(t,h))^2\, f_{X_0}\big(y(x;t,h)\big)\, \phi\big(y(x;t,h)\big)\,\mathrm{d}h, \tag{21}$$

where

$$\phi(y) := \frac{\alpha-1}{y} - \frac{\beta-1}{1-y}. \tag{22}$$

All prefactors in the integrand of (21) are nonnegative. Consequently, the sign of $\frac{\mathrm{d}}{\mathrm{d}x} f_{X_A}(x,t)$ is entirely determined by the function $\phi(y)$. The qualitative behavior of the PDF therefore depends on the parameters $\alpha > 0$ and $\beta > 0$, leading to the following cases:

- **Case 1 ($\alpha, \beta > 1$).** In this case, the function

$$\phi(y) = \frac{\alpha-1}{y} - \frac{\beta-1}{1-y} = \frac{(\alpha-1)(1-y) - (\beta-1)y}{y(1-y)}$$

is well defined on $(\varepsilon, 1-\varepsilon)$. Since the denominator is strictly positive, the sign of $\phi(y)$ is determined by the affine numerator

$$N(y) := (\alpha-1) - (\alpha+\beta-2)y.$$

The function $N(y)$ has negative slope and vanishes at the unique point

$$y^\star = \frac{\alpha-1}{\alpha+\beta-2} \in (\varepsilon, 1-\varepsilon),$$

so that $\phi(y) > 0$ for $y < y^\star$ and $\phi(y) < 0$ for $y > y^\star$.

For fixed $t > 0$ and $h \in (0, T)$, the mapping

$$x \longmapsto y(x;t,h) = x g_1(t,h) - g_2(t,h)$$

is affine and strictly increasing. For sufficiently small values of t, one has $g_1(t,h) \to 1$ and $g_2(t,h) \to 0$ uniformly in h, so that $y(x;t,h)$ is a small perturbation of the identity. As a consequence, there exists a unique value $x^\star(t)$ such that

$$y(x^\star(t);t,h) \approx y^\star \quad \text{for all } h \in (0,T),$$

up to higher–order terms in t.

Using (21), it follows that the sign of $\frac{\mathrm{d}}{\mathrm{d}x} f_{X_A}(x,t)$ changes exactly once at $x = x^\star(t)$: it is positive for $x < x^\star(t)$ and negative for $x > x^\star(t)$. Therefore, for small times t, the PDF $f_{X_A}(\cdot,t)$ admits a unique interior critical point, which is a global maximum. This maximum represents the most probable active–state fraction at time t, corresponding to the value around which the stochastic dynamics concentrate when the influence of the initial condition is still significant. In this regime, the shape of the PDF is primarily inherited from the initial distribution and only weakly distorted by the randomness in the cycle length.

For large values of t, the dependence on the initial condition is progressively lost. The set of x for which $y(x;t,h) \in (\varepsilon, 1-\varepsilon)$ for a non-negligible range of h becomes increasingly narrow, and the contribution of f_{X_0} acts only as a localized weight. In this regime, the shape of $f_{X_A}(\cdot,t)$ is primarily dictated by the distribution of H and

the Jacobian factor $g_1(t,h)$, which is consistent with the deterministic asymptotic behavior observed numerically.

Finally, we note that intermediate values of t do not require a separate analysis. Under the present assumptions, the mapping

$$t \longmapsto f_{X_A}(\cdot, t)$$

depends continuously on t, since the functions $g_1(t,h)$ and $g_2(t,h)$ vary smoothly with time and differentiation under the integral sign is justified. As a consequence, changes in the number or nature of critical points would require degenerate configurations, which are excluded here. Therefore, the qualitative structure of the PDF evolves continuously from the small–t regime, where it reflects the shape of the initial distribution X_0, to the large–t regime, where it is predominantly governed by the statistics of the random light–dark cycle.

- **Case 2 ($\alpha > 1$, $\beta \leq 1$).** In this regime, the function $\phi(y)$ is nonnegative on $(\varepsilon, 1-\varepsilon)$. Indeed, the term $(\beta-1)/(1-y)$ is non-positive, while $(\alpha-1)/y > 0$. Consequently, the integrand in (21) is nonnegative wherever it is nonzero, and

$$\frac{\mathrm{d}}{\mathrm{d}x} f_{X_A}(x,t) \geq 0 \quad \text{on the effective support.}$$

  Therefore, $f_{X_A}(\cdot,t)$ is monotonically increasing and admits no interior critical points. The maximum is attained at the upper boundary of its effective support, corresponding to values of x for which $y(x;t,h)$ approaches $1-\varepsilon$.

- **Case 3 ($\alpha \leq 1$, $\beta > 1$).** This case is symmetric to Case 2. The function $\phi(y)$ is non-positive on $(\varepsilon, 1-\varepsilon)$, since $(\alpha-1)/y \leq 0$ and $(\beta-1)/(1-y) > 0$. As a result,

$$\frac{\mathrm{d}}{\mathrm{d}x} f_{X_A}(x,t) \leq 0 \quad \text{on the effective support,}$$

  and the PDF is monotonically decreasing. No interior critical points exist, and the maximum is attained at the lower boundary of the effective support, corresponding to $y(x;t,h) \to \varepsilon$.

- **Case 4 ($\alpha, \beta < 1$).** In this case, the Beta density is U–shaped on $(0,1)$ and remains strictly convex on the truncated interval $(\varepsilon, 1-\varepsilon)$. The function $\phi(y)$ changes sign from negative to positive, vanishing at a unique point in $(\varepsilon, 1-\varepsilon)$. Accordingly, $\frac{\mathrm{d}}{\mathrm{d}x} f_{X_A}(x,t)$ changes sign from negative to positive, and $f_{X_A}(\cdot,t)$ admits a single interior minimum but no interior maxima. The distribution therefore concentrates near the boundaries of its effective support, reflecting strong variability in the initial active–state fraction.

When $\alpha = \beta = 1$, the initial condition X_0 is uniformly distributed on $[\varepsilon, 1-\varepsilon]$. In this case, the density f_{X_0} is constant on its support and vanishes elsewhere, so that $\frac{\mathrm{d}}{\mathrm{d}y} f_{X_0}(y) = 0$ for $y \in (\varepsilon, 1-\varepsilon)$. As a consequence, the integrand in (21) vanishes wherever it is nonzero, and therefore $\frac{\mathrm{d}}{\mathrm{d}x} f_{X_A}(x,t) = 0$ on the interior of the effective support.

Hence, the PDF $f_{X_A}(\cdot, t)$ is flat on its interior support and admits no interior critical points; any extrema can only occur at the boundaries of the effective support induced by the transformation $y(x; t, h) = xg_1(t, h) - g_2(t, h)$. This configuration does not introduce new qualitative behaviors, but rather serves as a neutral reference case in which the shape of the PDF is determined entirely by the random light–dark forcing and the associated transformation, without preferential weighting from the initial condition. For this reason, the uniform case provides a natural baseline for the numerical experiments presented in Section 4, where it is used to isolate the effect of the stochastic cycle period H on both instantaneous and averaged observables.

From a biological perspective, the above classification in Cases 1-4 highlights how variability in the initial activation state of photosystems influences population–level behavior under stochastic light forcing. When the initial distribution is unimodal ($\alpha, \beta > 1$), the system exhibits a single most probable active–state fraction at finite times, indicating robust concentration around a dominant physiological regime. In contrast, monotonic or U–shaped initial distributions reflect strong heterogeneity, leading to boundary–dominated or effectively bimodal tendencies that persist until the system reaches its long–time regime. Importantly, the loss of sensitivity to the initial condition at large times mirrors the experimentally observed "memory loss" in photosynthetic dynamics, whereby long–term productivity is controlled primarily by the statistics of the light–dark cycle rather than by transient initial states. This analytical insight clarifies the mechanisms through which environmental variability shapes phenotypic heterogeneity and robustness in photosynthetic populations.

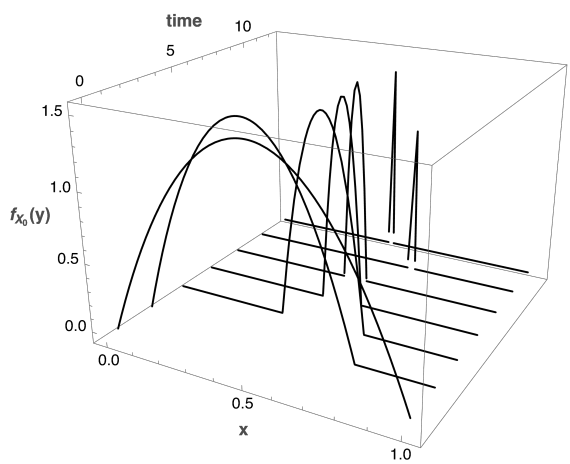


Fig. 4: PDF of the transferred initial condition f_{X_0} evaluated at $y = xg_1(t, h) - g_2(t, h)$ for $x \in [\varepsilon, 1 - \varepsilon] \subset (0, 1)$ with $\varepsilon = 0.001$ and times $t = 1, \ldots, 10$ with $\alpha = \beta = 2$, $h = 5$, and $r = 0.5$. All other model parameters as described in Table 1. The plot illustrates the progressive concentration of the probabilistic density as time increases tending to a leptokurtic shape.

3.3. Randomized Average Growth Rate

While the instantaneous state variable $X_A(t)$ provides detailed information on photosynthetic dynamics, long-term performance is more naturally characterized through time-averaged quantities. In particular, the average growth rate constitutes a macroscopic indicator of productivity that integrates intracellular dynamics with environmental variability. When the light–dark cycle length is random, this averaged quantity becomes itself a random variable, whose distribution reflects how fluctuations in the external regime are transmitted to biomass production.

Assuming that H and X_0 are independent random variables, the growth rate defined in Eq. (8) becomes a random variable. As established in the deterministic setting and extended here pathwise, for almost every realization $\omega \in \Omega$ there exists a finite transient time $t^\star(\omega) < \infty$ such that the trajectory $X_A(t, H(\omega))$ reaches a quasi-steady regime for all $t > t^\star(\omega)$. We assume that there exists a deterministic constant $s < \infty$ such that

$$X_A(t, H(\omega)) \text{ is in the quasi-steady regime for all } t \geq s, \text{ almost surely.}$$

To ensure that the averaging interval lies entirely within this regime for all realizations, we assume that the random cycle length H is bounded away from zero, namely

$$H(\omega) \in [\delta, T), \quad \delta > 0,$$

and choose an integer $K \in \mathbb{N}$ such that

$$K\delta > s.$$

Under this condition, the interval $(KH(\omega), (K+1)H(\omega))$ is contained in the quasi-steady regime almost surely.

We then define the random average growth rate, analogously to its deterministic counterpart, as

$$M(r; H) := \frac{\kappa\gamma}{H} \int_{KH}^{(K+1)H} X_A(t, r; H)\, \mathrm{d}t, \qquad r \in (0, 1), \tag{23}$$

where r denotes the light fraction of each cycle and is treated as a deterministic control parameter, while randomness enters exclusively through H. Although the definition of $M(r; H)$ involves the explicit solution of the reduced PSF model, once the quasi–steady regime is reached, X_0 does not influence the variability of M, which is driven entirely by the random cycle length H.

For fixed r, the mapping $H \mapsto M(r; H)$ defines a real-valued random variable. To compute its PDF, we take advantage of the RVT approach used previously for the derivation of the 1-PDF of $X_A(t)$. Let the vector of independent random variables be $\boldsymbol{u} := (X_0, H)$, and define the transformation $\boldsymbol{p} : \boldsymbol{u} \mapsto \boldsymbol{v} := (M, H)$ by $\boldsymbol{p} = (p_1, p_2)$, where p_1 is given by Eq. (23) and p_2 is the identity on H. Using the explicit solution of the reduced PSF model, the inverse mapping $\boldsymbol{s} := \boldsymbol{p}^{-1} = (s_1, s_2)$ is given by

$$\boldsymbol{s}(M, H) = \left(\frac{1}{I_2(H)} \left(\frac{HM}{\kappa\gamma} - I_1(H) \right),\ H \right), \tag{24}$$

where

$$I_1(H) := \int_{KH}^{(K+1)H} {g_1}^{-1}(t,H)\left(\int_0^t g_1(t,H)\, b(s,u(s;H))\,\mathrm{d}s\right)\mathrm{d}t,$$

$$I_2(H) := \int_{KH}^{(K+1)H} {g_1}^{-1}(t,H)\,\mathrm{d}t.$$

Since $\nu(t,u(t;H)) > 0$ for all t and almost every H, it follows that $I_2(H) > 0$ almost surely, and the transformation is invertible. The determinant of the Jacobian of the inverse mapping is therefore

$$\left|\frac{\partial s_1}{\partial M}\right| = \frac{H}{\kappa\gamma I_2(H)} \neq 0, \quad \text{almost surely.}$$

Then, the PDF of the random growth rate M is given by

$$f_M(\mu) = \int_{\mathbb{R}} f_H(h)\, f_{X_0}\left(\frac{1}{I_2(h)}\left(\frac{h\mu}{\kappa\gamma} - I_1(h)\right)\right)\left|\frac{h}{\kappa\gamma I_2(h)}\right|\mathrm{d}h. \tag{25}$$

For numerical efficiency, the integrals defining $I_1(h)$ and $I_2(h)$ are evaluated using the piecewise decomposition introduced in Eqs. (17)–(18), which exploits the piecewise-constant structure of the irradiance and avoids repeated integrations over random time partitions. Equivalently, the PDF of M can be expressed in expectation form as

$$f_M(\mu) = \mathbb{E}_H\left[f_{X_0}\left(\frac{1}{I_2(H)}\left(\frac{H\mu}{\kappa\gamma} - I_1(H)\right)\right)\left|\frac{H}{\kappa\gamma I_2(H)}\right|\right], \tag{26}$$

which is particularly convenient for Monte Carlo or quadrature-based numerical evaluations.

The distribution of the randomized average growth rate $M(r;H)$ provides a macroscopic synthesis of the stochastic dynamics analyzed in the previous section. Once the system has entered the quasi-steady regime, the averaging over complete light–dark cycles suppresses any persistent influence of the initial physiological state, so that variability in M is driven primarily by fluctuations in the cycle length H. This behavior is consistent with the asymptotic properties of the PDF of $X_A(t)$, where the dependence on X_0 was shown to vanish over time and the distribution to concentrate under the action of the random light–dark forcing. From a biological perspective, this indicates that short-term heterogeneity in photosystem activation acts as a fast, stabilizing mechanism, while long-term variability in productivity is controlled by the statistics of the external environment. As a consequence, populations subjected to fluctuating hydrodynamic conditions may exhibit substantial dispersion in growth rates even when their intracellular regulatory dynamics are tightly constrained.

4. NUMERICAL EXPERIMENTS

After establishing the 1-PDF of the proportion of active cells, $X_{\mathrm{A}}(t;H)$, in Eq. (16), and the PDF of the growth rate M in Eq. (25), we now illustrate the framework with a series of numerical examples.

To simulate realistic initial conditions, we assume the system starts near complete darkness, setting $X_0 \sim U(\varepsilon, 0.01)$, $\varepsilon = 0.001$ (i. e., the proportion of active cells is restricted to the interval $(\varepsilon, 0.01)$). While a delta distribution centered at zero could also be used to represent a deterministic initial condition, achievable by keeping the PSF in darkness for a sufficiently long time, we opt for the uniform distribution for modeling convenience. This choice offers a reasonable approximation of the deterministic case while maintaining analytical tractability.

To investigate how the random variable H affects the average growth rate M defined in (23), we define the normalized productivity:

$$P(H, r) := \frac{M(H, r)}{\mu_o(u_{\mathrm{av}})}, \tag{27}$$

as derived from randomizing Eq. (9). We explore various distributions for H, each centered around the experimental value $h_e = 45\,\mathrm{s}$. Other experimental parameters include the irradiance $I_e = 220\,\mu\mathrm{E\,m^{-2}\,s^{-1}}$, the calibrated parameters from Table (1) (as described in [25]), and a light-dark cycle ratio $r = 0.5$, indicating equal durations of light and darkness. All simulations assure that $\mathbb{P}[0 < H < e^4] \approx 0$.

Numerical experiments are performed using *Mathematica* [11], with 5 000 random samples of X_0 and H.

We consider three families of probability distributions for H, summarized in Table 2.

ID	Distribution	Expression
(1)	Uniform	$U(h_e - \sqrt{0.15\,h_e},\, h_e + \sqrt{0.15\,h_e})$
(2)	Normal	$\mathcal{N}(h_e,\, 0.05\,h_e)$
(3)	Bimodal	$\mathrm{MixtureModel}\left(\mathcal{N}(h_e \pm \sqrt{0.05\,h_e - 1},\, 1),\, \left\{\frac{1}{2},\, \frac{1}{2}\right\}\right)$

Tab. 2: Distributions of H used in the numerical simulations.

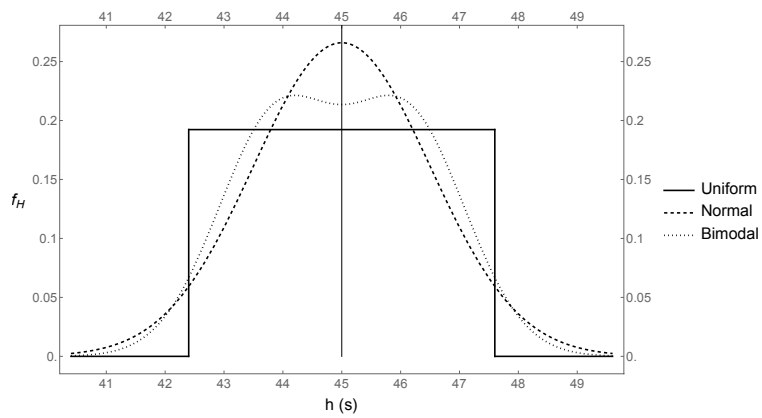


Fig. 5: Probability density functions (1)–(3) of H as defined in Table 2.

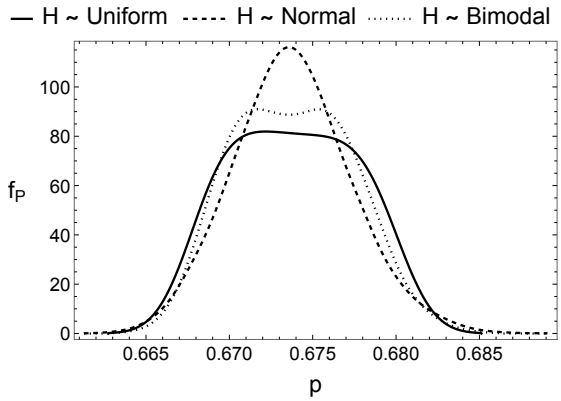


Fig. 6: PDF of P when H is distributed as described by (1)–(3).

Comparison	Cramér–von Mises p-value	Kolmogorov–Smirnov p-value
Uniform vs Normal	3.88×10^{-13}	3.55×10^{-15}
Uniform vs Bimodal	0.001563	5.71×10^{-4}
Normal vs Bimodal	4.87×10^{-6}	8.24×10^{-6}

Tab. 3: Pairwise goodness-of-fit test p-values for the distributions of P under different H distributions ((1)–(3)). Null hypothesis: the two samples come from the same distribution.

Despite all three distributions of H having the same mean and variance, the resulting distributions of P are distinct, as can be seen in Figure 6, where we can clearly see the influence of the shape of the PDF of H. Specifically, we find:

$$\mathbb{E}[P] \approx 0.6738, \quad \mathbb{V}[P] \approx 1.223 \times 10^{-5}$$

for all three cases. However, the low p-values from both the Cramer-von Mises and Kolmogorov-Smirnov statistical tests summarized in Table 3 provide strong evidence to reject the null hypothesis, confirming that the shape of the distribution of H significantly influences the shape of the distribution of P, even though the mean and variance remain unchanged.

These results highlight the critical role of the distributional shape of H in determining the behavior of the normalized productivity P. Although the mean and variance of H are held constant across all cases, the resulting PDFs of P differ significantly, as confirmed by statistical tests. This demonstrates that higher-order characteristics of H, such as skewness, modality, and tail behavior, can substantially influence the distribution of P, underscoring the necessity of carefully selecting or modeling the PDF of H when predicting or optimizing system performance. Therefore, having experimental evidence or direct measurements of the PDF of H would be valuable, as it would allow for more accurate and reliable modeling of productivity outcomes in real-world scenarios.

4.1. Analysis of the 1-PDF of $X_A(t)$ and the PDF of P for specific distributions

The 1-PDF of the stochastic process $X_{\mathrm{A}}(t;H)$ is given by the closed-form expression in Eq. (16). Since the original deterministic reduced model is a linear differential equation, this formulation directly relates the solution process $X_A(t;H)$ to the initial condition X_0 and the random cycle period H. Numerical approximations are only necessary for the integrals within the expression, specifically ν. We have leveraged the direct relationship between the solution and the initial condition to get the 1-PDF in a reliable manner. Figure 7 shows the distribution of the proportion of active photosynthetic units, given in (16), at different time instants $t = \{1, 1.1, 1.3, 1.6, 2\}$ minutes, using a light/dark ratio of $r = 0.5$. For these computations, the randomized cycle period H is assumed a truncated Gaussian distribution, $H \sim \mathrm{N}_{T=[0,1.5]}(\frac{45}{60} = 0.75 \text{ minutes}, \sqrt{0.75 \cdot 0.05})$, and the initial condition is uniformly distributed $X_0 \sim \mathrm{U}(0, 0.1)$.

The distribution is generally unimodal, reflecting the expected behaviour of the active state proportion under a periodic input. However, its shape and position vary over time due to the influence of the random cycle period H. Notably, the peak occurs near the mean. The spread, or variance, of the 1-PDF at different time instants illustrates how the uncertainty in the cycle period H propagates through the system and affects the instantaneous proportion of active photosynthetic units $X_A(t)$.

In Subsection 3.3, the PDF of the growth rate $M(r;H)$ has been derived, see Eq. (25). This expression is a convolution of the initial condition PDF and the terms resulting from the integral of the solution over one cycle in the quasi-steady state regime, weighted by the PDF of the random variable H. For efficient numerical computation, the integrals are decomposed based on the piecewise constant nature of the irradiance.

Although $M(r;H)$ characterizes the averaged system response under stochastic forcing, it retains physical units and depends on multiplicative structural parameters. For this reason, it is convenient to consider the normalized productivity defined in (27), which is dimensionless and independent of trivial scaling effects. This normalization isolates the influence of the random input H and allows the uncertainty propagation to be analyzed in relative terms. Since P is obtained from M through a linear scaling transformation, its PDF follows directly from Eq. (25) as

$$f_P(p) = \mu_o(u_{av})\, f_M(\mu_o(u_{av})\, p)\,, \tag{28}$$

where f_M denotes the PDF of M. In Figure 8 the PDF of P has been presented for $r = 0.5$ and using the same distributions for H and X_0, previously indicated. The parameter $K = 3$ ensures that the averaging interval lies within the quasi-steady state regime for this example. We observe that the PDF of P is unimodal, approximately symmetric, and concentrated around its mean value, indicating that most realizations of the random cycle period lead to very similar productivity levels. The relatively narrow spread of the distribution reflects a limited variability of the normalized productivity, suggesting that the system responds in a stable manner to moderate fluctuations in the light–dark cycle length. A slight asymmetry can be observed, reflecting the nonlinear dependence of productivity on the cycle length. Moreover, the distribution lies almost entirely below one, confirming that stochastic light–dark cycling rarely exceeds the productivity achieved under constant optimal illumination. Specifically, with an

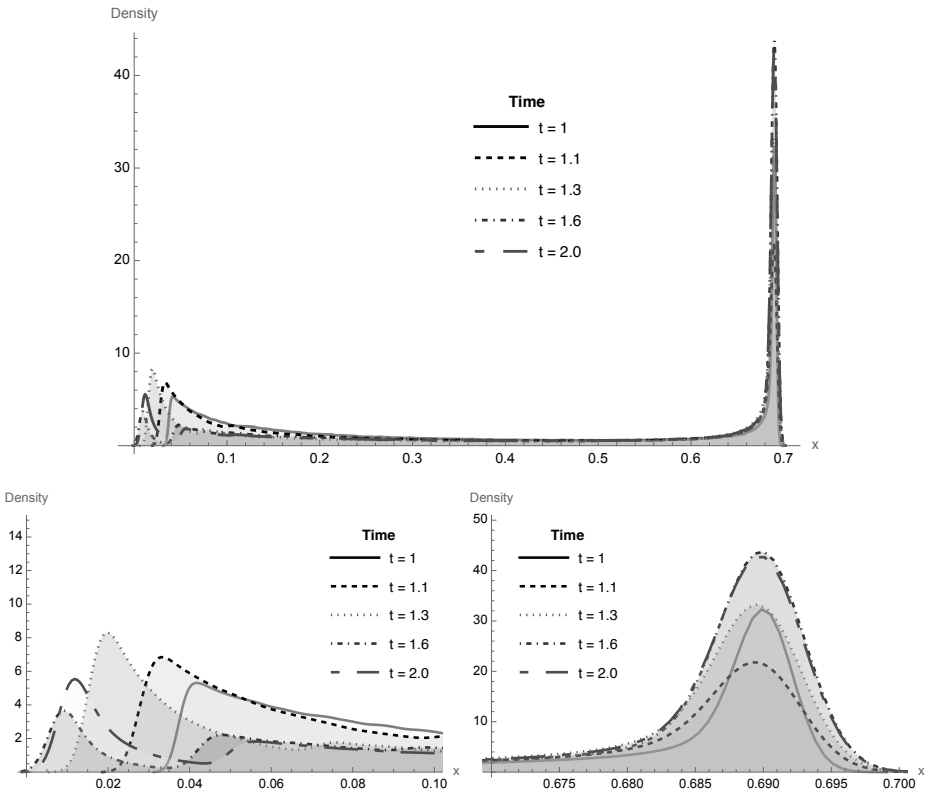


Fig. 7: Top: 1-PDF of the solution stochastic process $X_A(t;H)$ given in (16) at the time instants $t = \{1, 1.1, 1.3, 1.6, 2\}$ with a light/dark ratio $r = 0.5$. The curves illustrate the evolution and the propagation of uncertainty induced by the random cycle period H. Bottom: Detail of the tails of the $X_A(t;H)$ 1-PDF. The probability accumulation evidences the sensitivity of the system to extreme realizations of the random cycle period H.

average productivity of $\mathbb{E}[P] \approx 0.7705$, a variance of $\mathbb{V}[P] \approx 0.0014$ and a 95% confidence interval of $IC_{95} = [0.7116, 0.8581]$, these results do not reflect the performance of flashing-light experiments, which have been shown to match or exceed continuous light productivity while significantly reducing energy consumption and cooling costs [1]. From a biological perspective, this means that environmental variability does not generate systematic productivity gains, but instead induces small deviations around a predominantly suboptimal yet stable growth regime.

The PDF provides a complete quantification of uncertainty for the primary performance indicator (the productivity), allowing researchers to determine not just the expected value, but also the probability of the productivity falling within a desirable range, which is crucial for the design and analysis of photobioreactors under variable conditions.

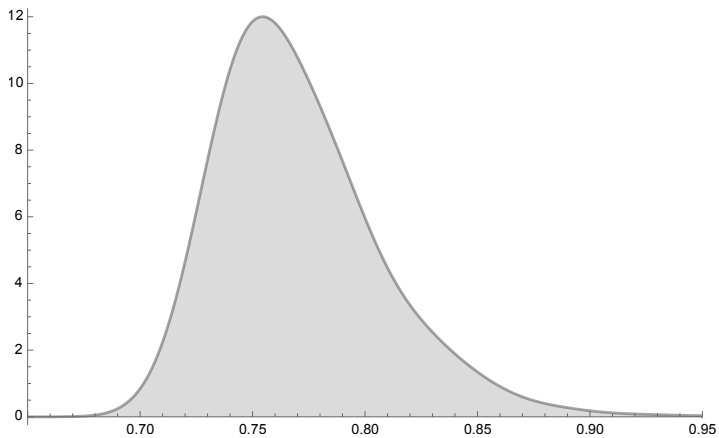


Fig. 8: PDF of the productivity P, given by (25) and (28), computed in the quasi-steady state regime using $K = 3$ averaging cycles and a light/dark ratio $r = 0.5$.

This analysis transforms a linear deterministic model into a probabilistic perspective that describes how fluctuations in the light cycle and the initial condition affect the behaviour of the microalgae growth.

5. CONCLUSIONS

In this work, we have investigated the growth dynamics of microalgae under light/dark cycles whose frequency is modeled as a continuous random variable. Specifically, by extending the deterministic Photosynthetic Factory (PSF) model in a Random Differential Equation (RDE) framework, we have incorporated randomness through the frequency of the light/dark cycles. This approach allowed us to derive the probability density functions (PDFs) for key system states, such as the proportion of active photosynthetic units, and also for the resulting growth rate. Our study highlights several findings related to the photosynthetic system. Even mild levels of randomness in the frequency F (or the period $H = 1/F$) can significantly affect both the short- and long-term behavior of the system. The distribution choice for the initial condition X_0, however, only affects the short-term dynamics of the system. Furthermore, we have shown that the choice of distribution of the period H influences the behavior of the random growth rate (whereas the random initial condition has no influence). A deeper understanding of the light period H, guided by real-life data and/or simulations, will, in turn, provide greater insight into the system's productivity the appropriate choice of distribution for H.
In this study, we have considered the light/dark period length H as an independent random variable with a predetermined distribution. This modelling choice captures uncertainty in the characteristic frequency of the light/dark cycles while preserving the analytical tractability required by the RVT-based framework developed in this work. However, it does not account for temporal correlations between successive light/dark cycles that may arise from turbulent mixing and other hydrodynamic effects. A more

realistic description of the fluctuating light environment experienced by individual cells would therefore involve modelling H (or equivalently the frequency F) as a stochastic process. Such an extension would require the development of alternative analytical and computational tools beyond the finite-dimensional random-variable setting considered here, and constitutes an interesting direction for future research. A natural extension would be to treat H (or the frequency F) as a stochastic process, possibly with time correlations or dependence on other environmental variables. Additionally, while we have focused on the "fast" reduced model and the average growth rate, other indicators of efficient cultivation could be studied. It would also be interesting to explore the long-term dynamics of the "full" random PSF model. Such approaches could lead to more comprehensive insights into the interplay between mixing-induced intermittent lighting and microalgal growth, ultimately guiding the design of more energy-efficient photobioreactors in industrial applications. Furthermore, given enough data of a species and its optimal flashing light regime setup, the approach we present in this study could be applied to take into account variability for optimization of algal growth.

ACKNOWLEDGEMENT

This work has been partially supported by the grant PID2025-172735NB-I00 funded by MICIU/AEI/10.13039/501100011033 and by the grant CIPROM/2026/22 funded by the Generalitat Valenciana (Conselleria de Educación, Cultura, Universidades y Empleo).

(Received March 9, 2026)

REFERENCES

[1] S. Abu-Ghosh, D. Fixler, Z. Dubinsky, and D. Iluz: Flashing light in microalgae biotechnology. Bioresource Technol. *203* (2016), 357–363.

[2] C. Andreu-Vilarroig, J. C. Cortés, and A. Navarro-Quiles, et al.: A random differential equation approach for modeling the growth of microalgae in photobioreactors. Bull. Math. Biol. *88* (2026), 47. DOI:10.1007/s11538-026-01609-3

[3] C. Brindley, N. Jiménez-Ruíz, F. G. Acién, and J. M. Fernández-Sevilla: Light regime optimization in photobioreactors using a dynamic photosynthesis model. Algal Res. *16* (2016), 399–408. DOI:10.1016/j.algal.2016.03.033

[4] G. Casella and R. L. Berger: Statistical Inference. Second edition. Duxbury, England 2002.

[5] S. Čelikovský, Š. Papáček, A. Cervantes-Herrera, and J. Ruiz-Leon: Singular perturbation based solution to optimal microalgal growth problem and its infinite time horizon analysis. IEEE Trans. Automat. Control *55* (2010), 3, 767–772. DOI:10.1109/TAC.2010.2040498

[6] A. Chiarini and M. Quadrio: The light/dark cycle of microalgae in a thin-layer photobioreactor. J. Appl. Phycol. *33* (2021), 183–195. DOI:10.1007/s10811-020-02310-1

[7] P. H. C. Eilers and J. C. H. Peeters: A model for the relationship between light intensity and the rate of photosynthesis in phytoplankton. Ecol. Model. *42* (1988), 199–215. DOI:10.1016/0304-3800(88)90057-9

[8] I. S. Gradshteyn and I. M. Ryzhik: Table of Integrals, Series, and Products. Seventh edition. Academic Press, Amsterdam 2007.

[9] C. Inostroza, L. Papáček, J. M. Fernández-Sevilla et al.: Optimization of thin-layer photobioreactors for the production of microalgae by integrating fluid-dynamic and photosynthesis rate aspects. J. Appl. Phycol. *35* (2023), 2111–2123. DOI:10.1007/s10811-023-03050-8

[10] M. Janssen: Cultivation of microalgae: effect of light/dark cycles on biomass yield. Dissertation, Wageningen Univ. 2002. Available at: https://edepot.wur.nl/121273.

[11] Mathematica: Wolfram Research, Inc. https://www.wolfram.com/mathematica/

[12] T. M. Mata, A. Martins, and N. S. Caetano: Microalgae for biodiesel production and other applications: A review. Renewable Sustainable Energy Rev. *14* (2010), 1. DOI:10.1016/j.rser.2009.07.020

[13] J. C. Merchuk, M. Ronen, S. Giris, and S. M. Arad: Light/dark cycles in the growth of the red microalga Porphyridium sp. Biotechnol. Bioengrg. *59* (2000), 6, 705–710.

[14] K. Mulluye, Y. Bogale, D. Bayle, and Y. Atnafu: Review on microalgae potential innovative biotechnological applications. Biosci. Biotechnol. Res. Asia *20* (2023), 1.

[15] T. Neckel and F. Rupp: Random Differential Equations in Scientific Computing. De Gruyter, Versita 2013.

[16] Š. Papáček, S. Čelikovský, D. Štys and J. J. Ruiz-León: Bilinear system as a modelling framework for analysis of microalgal growth. Kybernetika *43*, No. 1 (2007), 1–20.

[17] Š. Papáček, S. Čelikovský, B. Rehák, and D. Štys: Experimental design for parameter estimation of two time-scale model of photosynthesis and photoinhibition in microalgae. Math. Comput. Simul. *80* (2010), 1302–1309.

[18] S. Papáček, J. Jablonsky, and K. Petera: Advanced integration of fluid dynamics and photosynthetic reaction kinetics for microalgae culture systems. BMC Syst. Biol. *12* (2018), Suppl. 5, 93.

[19] B. Rehák, S. Čelikovský, and Š. Papáček: Model for Photosynthesis and Photoinhibition: Parameter Identification Based on the Harmonic Irradiation O_2 Response Measurement. Joint Special Issue of TAC IEEE and TCAS IEEE (2008), pp. 101–108.

[20] P. Rudnicki, X. Gao, B. Kong, and R. D. Vigil: A comparative study of photosynthetic unit models for algal growth rate and fluorescence prediction under light/dark cycles. Algal Res. *24* (2017), 227–236. DOI:10.1016/j.algal.2017.03.028

[21] T. T. Soong: Random Differential Equations in Science and Engineering. Academic Press, 1973.

[22] M. R. Tredici: Photobiology of microalgae mass cultures: understanding the tools for the next green revolution. Biofuels *1* (2010), 1, 143–162. DOI:10.4155/bfs.09.10

[23] C. Vejrazka et al.: Photosynthetic efficiency and oxygen evolution of *Chlamydomonas reinhardtii* under continuous and flashing light. Appl. Microbiol. Biotechnol. *97* (2013), 4, 1523–1532. DOI:10.1007/s00253-012-4390-8

[24] S.-K. Wang, A. R. Stiles, C. Guo, and C.-Z. Liu: Microalgae cultivation in photobioreactors: An overview of light characteristics. Engrg. Life Sci. *14* (2014), 6, 550–559. DOI:10.1002/elsc.201300170

[25] X. Wu and J. C. Merchuk: A model integrating fluid dynamics in photosynthesis and photoinhibition processes. Chem. Engrg. Sci. *56* (2001), 3527–3538. DOI:10.1016/S0009-2509(01)00048-3

Juan Carlos Cortés López, Instituto Universitario de Matemática Multidisciplinar, Universitat Politècnica de Valencia, Camino de Vera s/n, Valencia, 46022. Spain.
e-mail: jccortes@mat.upv.es

Ana Navarro-Quiles, Instituto Universitario de Matemática Multidisciplinar, Universitat Politècnica de Valencia, Camino de Vera s/n, Valencia, 46022. Spain.
e-mail: annaqui@upv.es

Štěpán Papáček, The Czech Academy of Sciences, Institute of Information Theory and Automation, Pod Vodárenskou věží 4, 182 08 Praha 8. Czech Republic.
e-mail: papacek@utia.cas.cz

Cristina Pérez Diukina, Instituto Universitario de Matemática Multidisciplinar, Universitat Politècnica de Valencia, Camino de Vera s/n, Valencia, 46022. Spain.
e-mail: cperdiu@upv.edu.es